Microporous and Mesoporous Materials 183 (2014) 134–142

Contents lists available at ScienceDirect

Microporous and Mesoporous Materials

journal homepage: www.elsevier.com/locate/micromeso

Morphological and structural evolution of mesoporous calcium aluminate nanocomposites by microwave-assisted synthesis

Yen-Po Chang, Po-Hsueh Chang, Yuan-Tse Lee, Tai-Jung Lee, Yen-Ho Lai, San-Yuan Chen *

Department of Materials Science and Engineering, National Chiao Tung University, Hsinchu 300, Taiwan

ARTICLE INFO

Article history:
Received 3 February 2013
Received in revised form 16 June 2013
Accepted 6 September 2013
Available online 17 September 2013

Keywords:
Metal oxides
Nanocomposites
Calcium aluminates
Microwave

ABSTRACT

Novel special dual-structure calcium aluminate nanocomposites consisting of mesoporous Ca-containing Al_2O_3 nanonetworks with $Ca_{12}Al_{14}O_{33}$ polycrystalline nanorods have been successfully synthesized using the microwave-hydrothermal (M-H) process in an alcohol solution consisting of calcium nitrate and mesoporous alumina, followed by calcination at a lower temperature (e.g., less than 600 °C). The mesoporous Ca-containing aluminate nanocomposites possessed a specific surface area of 51 $m^2\ g^{-1}$ and a broad pore size distribution of 4–12 nm in diameter, as observed from N_2 adsorption/desorption measurements. The results showed that highly dispersed $Ca_{12}Al_{14}O_{33}$ nanorods grown on the mesoporous nanostructure were obtained by varying the molar ratio of Ca/Al or by controlling microwave heating time, as characterized by scanning electron microscopy (SEM), transmission electron microscopy/electronic energy loss spectroscopy (TEM/EELS) and powder X-ray diffraction (PXRD). The $Ca_{12}Al_{14}O_{33}$ nanorods with diameters of 50–100 nm and lengths of 200–400 nm were grown in and on the one-dimensional mesochannels. A formation mechanism of the mesoporous Ca-containing aluminate nanocomposites involving amorphous mesoporous hydrated-Al_2O_3 was also proposed.

1. Introduction

Calcium aluminates ($Ca_{12}Al_{14}O_{33}$) have long been known as refractory mixed oxides in the steel industry and as hydraulic materials in the cement community. In recent years, new applications of calcium aluminates have emerged, such as optical devices [1], oxygen ionic conductors [2], and heterogeneous catalysts [3,4]. Lemonidou et al. reported that the deposition of 5 wt.% Ni on calcium aluminate (molar ratio $CaO/Al_2O_3 = 1/2$) resulted increased catalytic activity, with lower coke deposition for the reaction of CO_2 reforming of CH_4 [4]. Traditionally, bulk calcium aluminate cements have been obtained by fusing or sintering a mixture of CaO or $CaCO_3$ and alumina (Al_2O_3) at temperatures above 1400 °C, but these materials have very low specific surface areas (<1 m^2/g) [5]. Risbud et al. reported that amorphous calcium aluminate ($Ca_{12}Al_{14}O_{33}$) powders with high surface areas can be synthesized by calcining a mixture of aluminum and calcium precursors (such as organic metal or metal salts) below 900 °C [6,7]. On the other hand, crystalline calcium aluminate ($Ca_{12}Al_{14}O_{33}$) can also be obtained by evaporative decomposition of a solution made from calcium and aluminum nitrate precursors after heat-treatment at 900 °C [8]. Recently, Zawrah et al. further reported that nanosized calcium aluminate with particle size smaller than 50 nm can be successfully synthesized by thermal decomposition treatment above 1000 °C [9]. However, to date, calcium aluminate nanocrystallites with mesoporous structures, which are used as supports for catalysts and oxygen ion conductors, have not been investigated.

In recent years, microwave-enhanced chemistry has become increasingly important because it can utilize the inherent properties of liquids, solids, and their mixtures to convert microwave energy in situ into heat for promoting reactions [10,11]. Hence, microwave-assisted synthesis of mesoporous materials (such as MCM-41 and SBA-15) has attracted wide attention [12,13] because it offers many advantages such as homogeneous and simultaneous heating through the reaction cell, rapid nucleation and growth, and suppression of undesired phases. To the best of our knowledge, no systematical study has yet been conducted on the synthesis of mesoporous calcium aluminate nanocomposites by microwave-assisted processes. In this study, we used microwave-assisted synthesis combined with calcination treatment to produce a special dual-structure of polycrystalline nanorods and/or nanonetworks. It was found that the Ca/Al molar ratio plays important roles in the migration of ionic calcium species on the mesostructured surface as well as in the morphology evolution of mesostructured calcium aluminate grown with $Ca_{12}Al_{14}O_{33}$ nanorods–nanotube nanocomposites. Characterization techniques, including nitrogen

* Corresponding author. Address: Department of Materials Science and Engineering, National Chiao Tung University, 1001 Ta Hsueh Road, Hsinchu 300, Taiwan, ROC. Tel.: +886 3 5731818; fax: +886 3 574727.
E-mail address: sanyuanchen@mail.nctu.edu.tw (S.-Y. Chen).

1387-1811/$ - see front matter © 2013 Elsevier Inc. All rights reserved.
http://dx.doi.org/10.1016/j.micromeso.2013.09.013

adsorption, powder X-ray diffraction (PXRD), scanning electron microscopy (SEM) and transmission electron microscopy (TEM) with electron energy loss spectroscopy (EELS), were used to examine the crystal structure, morphology and size of nanostructured calcium aluminates. The formation mechanism of the nanostructure grown on the surface of mesoporous materials was proposed to explain the microwave reaction between calcium ion and mesoporous alumina.

2. Experimental section

2.1. Preparation of mesoporous calcium aluminate nanocomposites

First, according to a previous study [14], Yuan et al. reported highly ordered mesoporous alumina (MA) with high thermal stability. In a typical preparation, triblock copolymer $HO(CH_2CH_2O)_{20}(CH_2CH(CH_3)O)_{70}-(CH_2CH_2O)_2OH$ (2 g; Sigma–Aldrich, Mn = 5800, Pluronic P123) was dissolved in absolute ethanol (20 mL; Sigma–Aldrich, 99.5%) and stirred for 4 h at room temperature. In another solution, aluminum isopropoxide (AIP, 20 mmol; Sigma–Aldrich, 98+ wt.%,) was dissolved in nitric acid (3.2 mL; J.T. Baker, 70 wt.%) and absolute ethanol (10 mL). Then, the AIP solution was slowly added to the surfactant solution, and the mixed solution was vigorously stirred for 5 h and then transferred to an oven to evaporate the solvent at 60 °C for 3 days. The resulting powder was calcined at 700 °C for 4 h with a heating rate of 5 °C min^{-1} in an air flow and then cooled in a furnace to ambient temperature to give mesoporous Al_2O_3 (M-Al).

Second, the synthesized M-Al and calcium nitrate were used as starting materials. These materials, with a Ca:Al molar ratio of 1:1 and 2:1, were suspended in 100 mL of absolute alcohol solution at room temperature. Then, the solution was transferred to the TFM (tetrafluorometyl) reactor. The reactors with the suspensions were sealed and then placed on a turntable tube for uniform heating by a microwave-accelerated reaction system (model MARSTM, CEM Corporation, Matthews, NC, USA). The suspensions in the TFM vessel were heated at 80 °C for 1 h in a microwave oven with 1600 W of power. The precipitation suspended in the solution was rapidly dried at 50 °C in an oven overnight to remove the solvent. Finally, the resulting powders were calcined at 600 °C for 3 h with a heating rate of 2 °C min^{-1} in an air flow to give M-CaAl and M-2CaAl powders with the Ca:Al molar ratio of 1:1 and 2:1, respectively.

2.2. Characterization of materials

The resulting powders were characterized by performing XRD measurements (MAC Science MXP18AHF XRD, with CuK_a radiation source, λ = 1.5418 Å). SEM images of the sample were collected with a JEOL-6700 field-emission electron microscope at an accelerating voltage of 15 kV. TEM micrographs and electron diffraction patterns were recorded with a JEOL JEM-2100F electron microscope equipped with an Oxford energy-dispersive spectrometer

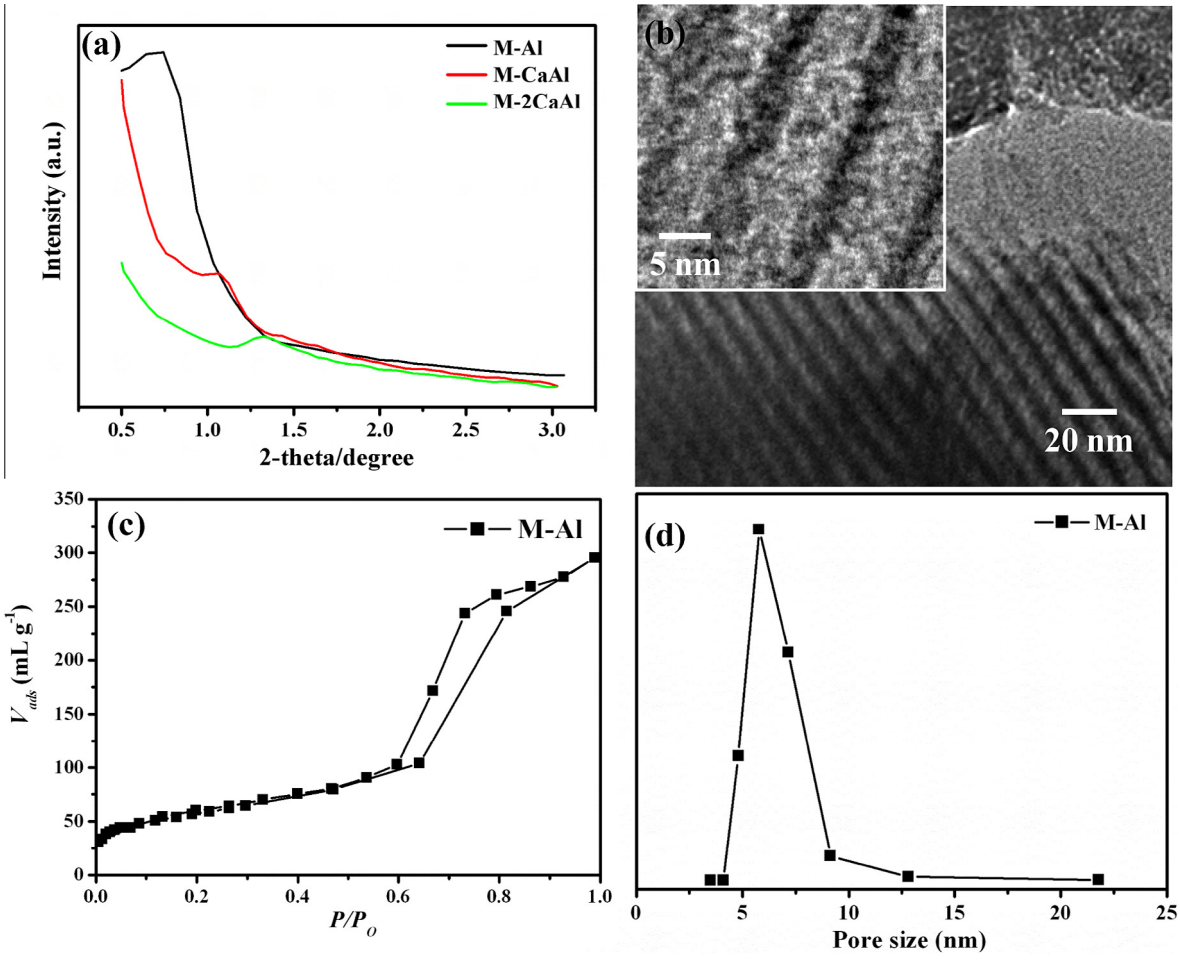

Fig. 1. (a) Small-angle XRD patterns, (b) TEM image with a high resolution image inset, (c) N_2 adsorption isotherm and (d) pore size distribution of calcined mesoporous Al_2O_3 (M-Al).

(EDS) analysis system. Elemental Ca or Al distribution mapping was conducted with a TECNAI 30 electron microscope fitted with an electron energy loss spectroscopy (EELS) detector. Samples for TEM measurements were embedded in resin and ultramicrotomed into slices with thicknesses of approximately 50 nm. The surface area (BET) and pore size distribution were calculated using a NOVA 1000e instrument at 77 K nitrogen adsorption isotherms. All samples were degassed under vacuum at 200 °C for 2 h prior to the measurements. The samples were digested with mixed acids and their Ca/Al ratios were determined by ICP-AES (Jarrell-Ash, ICAP-9000). The as-synthesized and calcined M-CaAl samples were also characterized by Fourier transform infrared spectroscopy (FTIR, Bomem DA8.3) and X-ray photoemission spectroscopy (XPS, Thermo VG Microlab 350).

3. Results and discussion

3.1. Mesoporous Al_2O_3

Fig. 1(a) illustrates the small-angle XRD patterns of mesoporous Al_2O_3 (M-Al), in which the characteristic reflections of the P6mm hexagonal structure at $2\theta = 0.79°$ (MA) are displayed and the corresponding d-spacing is indexed with $d_{100} = 11.18°$. The hexagonal unit cell parameter (a_o) of 12.9 nm (MA) was calculated by assuming a (100) reflection for the hexagonal array of pores of the mesoporous metal oxides, which is indicative of mesostructural formation. This finding also indicates that a hexagonal arrangement of the mesoporous structure was evolved upon mesoporous metal oxide synthesis. The large-angle XRD (LA-XRD) pattern of the M-Al sample is shown in Fig. 2(a). After calcination at 700 °C, mesoporous Al_2O_3 (M-Al) displays three broad peaks from the (311), (400), and (440) reflections, which correspond to those of crystalline γ-Al_2O_3 (JCPDS No. 29-1486), indicating a crystalline γ-Al_2O_3 framework. The high-resolution image of mesoporous Al_2O_3 in Fig. 1(b) exhibits channels with 2D-hexagonal symmetry (P6mm) along (110) with an interplanar space calculated as ~7.5 nm, in good agreement with that determined by SA-XRD. Nitrogen adsorption isotherms and the corresponding pore size distribution of mesoporous Al_2O_3 (M-Al) are shown in Fig. 1(c) and (d). The isotherms can be classified as type IV, indicating typical mesoporous metal oxides [15]. The hysteresis loop of M-Al displays type H1 characteristic and the steepness of the capillary condensation step indicate the uniformity of the mesopores. The Brunauer–Emmett–Teller (BET) surface areas, pore volumes and average pore size of the M-Al sample are measured to be 202 $m^2\ g^{-1}$; 0.47 $cm^3\ g^{-1}$; and 5.8 nm, respectively.

3.2. Mesoporous calcium aluminate nanocomposites

Mesoporous calcium aluminate nanocomposites with different molar ratios of M-CaAl and M-2CaAl were synthesized by reacting mesoporous Al_2O_3 with a controlled concentration of calcium under the microwave-assisted hydrothermal process in which the actual Ca/Al molar ratio of 0.96 (M-CaAl) and 1.94 (M-2CaAl) was measured by ICP-AES. The small- and large-angle XRD patterns of the calcined mesoporous nanocomposites (M-CaAl and M-2CaAl) are shown in Figs. 1(a) and 2(a), respectively. The small-angle XRD pattern of the M-CaAl and M-2CaAl samples displayed a single broad diffraction peak at $2\theta = 1.06°$ and $2\theta = 1.33°$, respectively. The pore size decreases with increasing molar ratio of Ca/Al, demonstrated by the reduction in d-spacing from 8 to 6.7 nm. However, the low intensity and broadness of the diffraction peak in the small-angle region indicate a wormhole framework, which reveals that Ca loading led to the amorphous structure. The existence of the small-angle diffraction peak also indicates the retention of

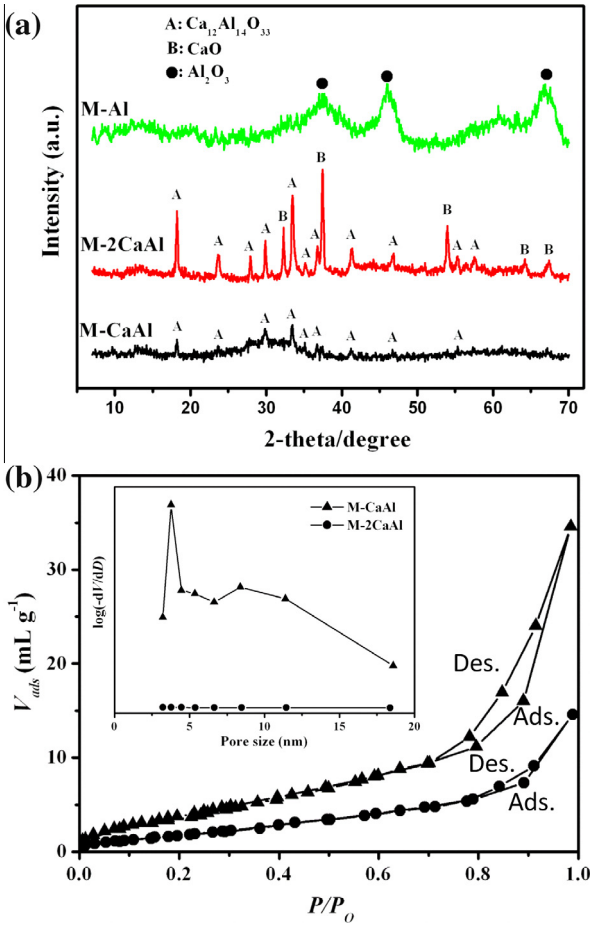

Fig. 2. (a) Large-angle XRD patterns and (b) N_2 adsorption isotherms and pore size distributions of calcined mesoporous materials.

the mesostructure throughout the calcination process [16]. This finding also demonstrates that the hexagonal arrangement of the mesoporous structure was evolved during the synthesis of the mesoporous calcium aluminates. Additionally, the large-angle XRD patterns of the M-CaAl (Ca/Al = 1:1) and M-2CaAl (Ca/Al = 2:1) samples that were calcined at 600 °C were characterized, and the main diffraction peaks correspond to crystalline structures of $Ca_{12}Al_{14}O_{33}$ (JCPDS No. 70-2144) and CaO (JCPDS No. 04-0777), marked as A and B, respectively. The visible diffraction peaks in the XRD pattern of the M-CaAl sample corresponded to the $Ca_{12}Al_{14}O_{33}$ crystalline phase and the broad peaks may also indicate the formation of mesoporous calcium-containing aluminates nanostructures in this compound. According to the previously reported literature, the $Ca_{12}Al_{14}O_{33}$ crystalline phase usually formed above 800 °C [17,18]. However, in our studies, this phase clearly appeared after calcinations at 600 °C. This difference may be attributed to the microwave heating because the microwave can directly interact with the dipole of molecules, resulting in accelerated uniform reactions. During the microwave heating, the generated thermal energy evenly distributes Ca ions in this reaction throughout the porous structure and induces a stronger affinity of the Ca ions to the highly active mesoporous Al_2O_3 matrix [19]; thus, the reactions between Ca and Al–O species could occur at lower temperatures to form mesoporous calcium-containing aluminate nanocomposites. Subsequently, the $Ca_{12}Al_{14}O_{33}$ polycrystalline phases could be grown from high-Ca concentration areas such as mesostructured surface and mesochannels during the calcination process. In addition, the XRD patterns of the M-2CaAl sample in Fig. 2(a) also show the formation of both CaO and $Ca_{12}Al_{14}O_{33}$ phases. It is implied

that the extra unreacted Ca species could be transferred to form calcium oxide after calcination at high temperature. Moreover, in Fig. 2(b), the mesoporous calcium-containing aluminate nanocomposites showed a hysteresis loop of type H2, which is typical for wormhole-like mesostructures and hierarchical scaffold-like mesoporous structures [20,21]. Some typical textural parameters of the M-CaAl and M-2CaAl samples were measured by Brunauer–Emmett–Teller (BET): specific surface area of 51 and 16 $m^2 g^{-1}$, pore volume of 0.09 and 0.04 $cm^3 g^{-1}$ and average pore size of 11.8 and 3.9 nm, respectively. These results indicate that an increase in Ca loading would cause the formation of excessive CaO particles, leading to partial blocking of the mesoporous system and thus a smaller BET surface area and pore volume in the M-2CaAl sample. In contrast, for a sample with less Ca (M-CaAl), Ca ions could be widely distributed throughout the mesoporous Al_2O_3 matrix to produce calcium-containing aluminate nanocomposites with larger BET surface area and pore volume after calcining the M-CaAl nanocomposites at 600 °C.

The SEM images of calcined mesoporous calcium-containing aluminate nanocomposites are displayed in Fig. 3. For the M-CaAl sample (Ca/Al = 1:1), Fig. 3(a) and (b) show that nanorods 200–400 nm in length and 50–120 nm in width were highly grown on the mesochannel and surface of the mesostructured matrix. The $Ca_{12}Al_{14}O_{33}$ nanorods seem to either directly nucleate and grow from the surface or initiate from the interior mesostructure. The energy-dispersive spectral analysis (EDS) in Fig. 3(c) and (d) also showed that no elements other than Ca, Al and O were detected, and the Ca/Al molar ratio of the mesoporous nanocomposites was estimated to be ca. 0.833 (spot 1) and ca. 0.892 (spot 2) based on the quantitative EDS analyses, possibly indicating that the mesoporous nanocomposites are characteristic of a highly chemically pure $Ca_{12}Al_{14}O_{33}$ phase. It is inferred that the

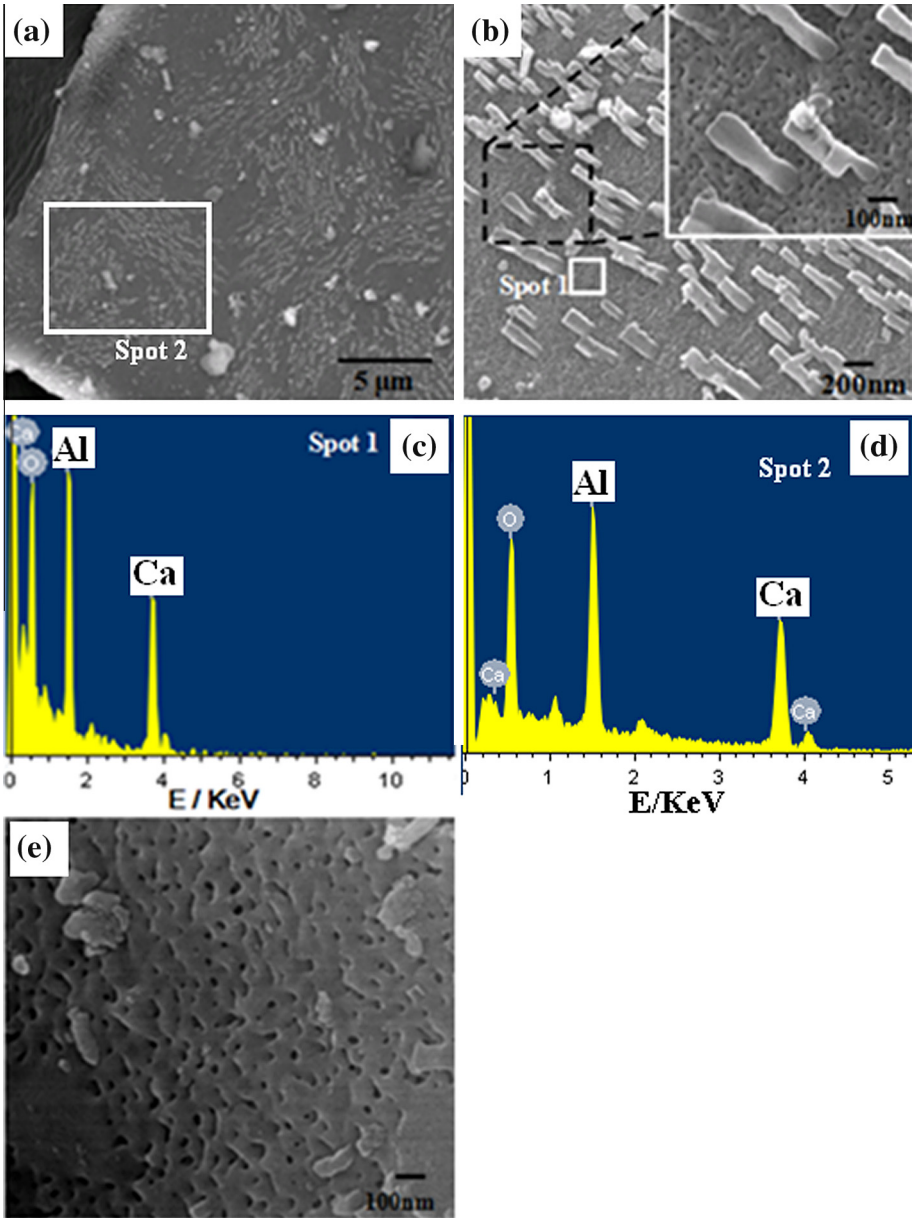

Fig. 3. SEM images of calcined M-CaAl samples, (a) at low magnification (2 K) and (b) high magnification (30 K), displaying nanorods grown on the surface of mesoporous oxide, (c) EDS from spot 1 in (b), (d) EDS from spot 2 in (a) and (e) SEM image of the M-2CaAl sample, presenting a mesoporous structure without nanorods. Note: the prepared M-CaAl sample with Ca/Al ratio = 1, and M-2CaAl sample with Ca/Al ratio = 2.

$Ca_{12}Al_{14}O_{33}$ nanorod-like crystallites on the mesoporous Ca-containing Al_2O_3 matrix were formed in situ from the calcinations and interactions of the Ca species and Al_2O_3 matrix hybrid precursor prepared by the microwave accelerated reaction. Moreover, a few particles (0.5–1.5 μm in size) also appeared on the surface of the mesoporous Ca-containing Al_2O_3 matrix, as shown in Fig. 3(a), which are attributed to the formation of calcium oxides due to unreacted calcium species on the Al_2O_3 matrix. In contrast, the M-2CaAl sample (Ca/Al = 2:1) in Fig. 3(e) displays a rougher surface morphology; no uniform nanorods can be detected, suggesting that the superabundant Ca species was possibly transferred into the aggregation of CaO particles on the mesoporous Ca-containing Al_2O_3 matrix, which is supported by the large-angle XRD results (as shown in Fig. 2(a)). Generally, pure $Ca_{12}Al_{14}O_{33}$ crystallites were formed at high temperature (up to 800 °C) by following the reaction of $12CaO + 7Al_2O_3 \rightarrow Ca_{12}Al_{14}O_{33}$ with Ca/Al molar ratio = 0.857; however, as excessive Ca was added, as in M-2CaAl (Ca/Al = 2), large CaO particles may have been easily formed on the mesostructural Al_2O_3 matrix after calcinations, as clearly evidenced by the sharp diffraction peaks of the CaO crystal phase in the XRD pattern.

The TEM images of the calcined calcium aluminate nanocomposites (M-CaAl and M-2CaAl samples) are shown in Figs. 4 and 5. For the M-CaAl sample, nanorods with diameter of 50–120 nm and length of 200–400 nm were distributed on the surface of the mesoporous Ca-containing Al_2O_3 matrix, as shown in Fig. 4(a). On the other hand, nanorods were observed growing outward from the pore structure inside a mesochannel in the magnified TEM image in Fig. 4(b), where the pore size distribution of the mesostructured matrix was ca. 10–50 nm. It is suggested that when the Ca species were loaded into the ordered mesoporous Al_2O_3 during microwave-assisted synthesis, a reaction between the mesoporous Al_2O_3 frameworks and the Ca ions could occur, forming an intermediate compound that was then transformed into the mesoporous calcium aluminates with $Ca_{12}Al_{14}O_{33}$ nanorods during the subsequent calcinations. During the synthetic process, the ordered mesoporous frameworks would be consumed, forming the larger mesopores. The high-resolution TEM (HRTEM) and FT (Fourier transform) diagram in Fig. 4(d) reveal that the nanorods are corresponding to $Ca_{12}Al_{14}O_{33}$ but seem to be poorly crystalline in structure because the indices of diffraction rings are consistent with the XRD peaks of the (211), (310), (321), and (420) reflections.

When the Ca/Al molar ratio was increased to 2, the TEM image of the M-2CaAl sample in Fig. 4(c) showed that no nanorods can be disclosed on the mesoporous frameworks, and the pore size distribution became non-uniform, with large nanopore sizes greater than 50 nm. Furthermore, most of the pores seem to be covered by excessive and large-scale CaO on the surface of the larger nanoporous calcium aluminates, limiting the growth of nanorods under calcinations at high temperature. Furthermore, TEM, EELS mapping, and FT (Fourier transform) diagrams were used to characterize the crystal structure and elemental distribution of the calcined mesoporous calcium aluminate nanocomposites (M-CaAl) in Fig. 5. The M-CaAl sample shows a mesoporous structure with nanorods forming the nanocomposites in Fig. 5(a). In addition, two images of the EELS mapping for Ca and Al were shown in Fig. 5(b) and (c), respectively. Fig. 5(d) is the overlapped image of Fig. 5(b) and (c), which can be clearly divided into two parts: (1) the Ca or Al atoms may be homogeneously dispersed in the mesoporous structure

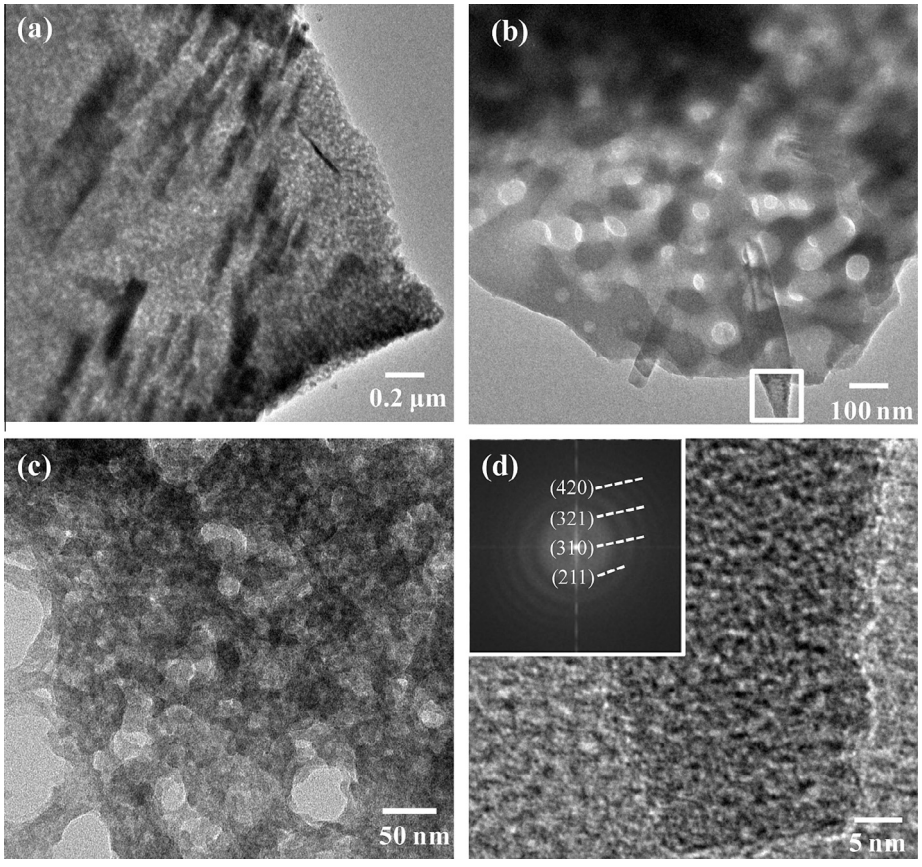

Fig. 4. TEM images of a calcined mesoporous M-CaAl sample, (a) at low magnification and (b) high magnification, displaying nanorods grown from inside a pore channel of mesoporous oxides, and (c) TEM images of a calcined mesoporous M-2CaAl sample. Image (d) shows the high resolution TEM image and FT pattern of the boxed area of M-CaAl in image (b). Note: the prepared M-CaAl sample with Ca/Al ratio = 1, and M-2CaAl sample with Ca/Al ratio = 2.

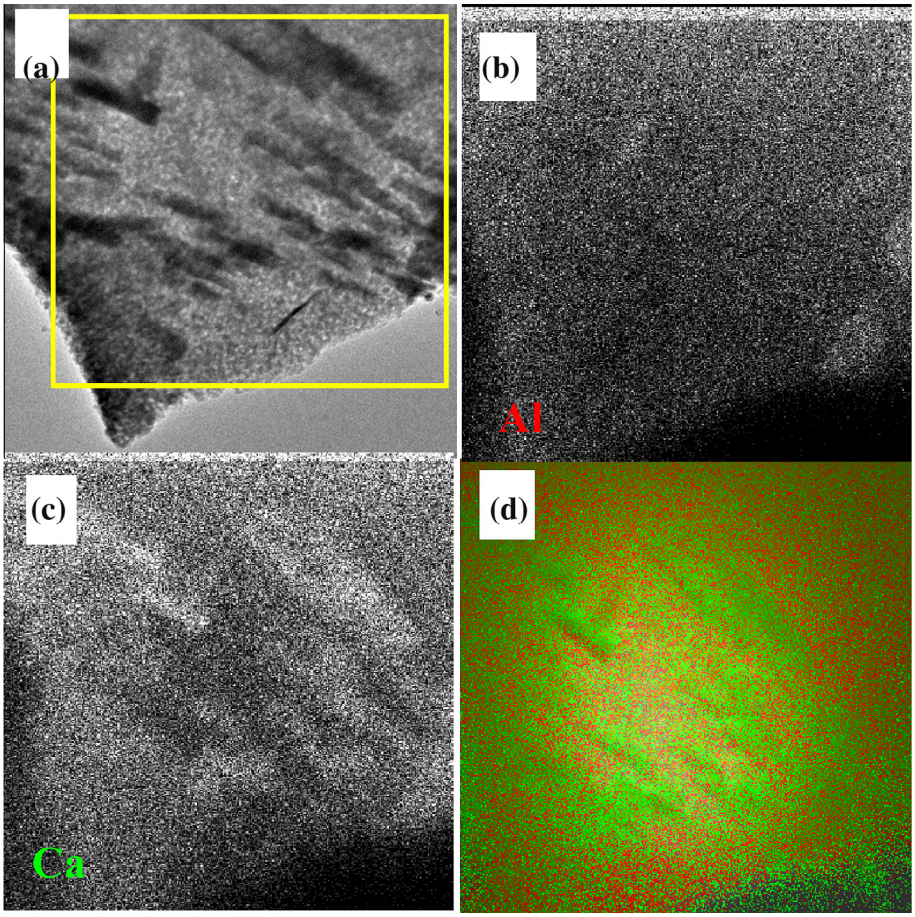

Fig. 5. (a) TEM image of the M-CaAl sample with Ca/Al ratio = 1, and the corresponding qualitative element mapping for (b) Al and (c) Ca by EELS analysis, (d) the overlap image of the (b) and (c) resulting images. (Note: green dots indicate Ca, and red dots indicate Al). (For interpretation of the references to color in this figure legend, the reader is referred to the web version of this article.)

with elemental compositions of Ca-containing Al_2O_3 frameworks; (2) the heterogeneous and aggregative Ca atoms are observed for $Ca_{12}Al_{14}O_{33}$ nanorods that grow either from the inside mesostructural channel or outside mesostructural surface. Hence, the $Ca_{12}Al_{14}O_{33}$ nanorods could be formed by a nucleation process between calcium species and mesoporous Al_2O_3, with subsequent growth in the later annealing process.

The Al 2s core level and valence band of the as-synthesized sample (after microwave hydrothermal treatment) and calcined sample (M-CaAl) were further analyzed using an XPS measurement. The XPS spectra in Fig. 6(a) indicate that the microwave-heated sample mainly displays the Al 2s of hydrated alumina (Al–OH and Al–OOH) at ~116 eV of binding energy. In contrast, the XPS spectrum of the calcined sample (M-CaAl) exhibited the Al 2s sharp peak at ~123 eV of binding energy, indicating the formation of calcium–aluminum oxides after calcination at high temperature. Further, the FTIR spectra of the as-synthesized and calcined samples (M-CaAl) in Fig. 6(b) evidenced the difference between microwave-assisted and calcined treatments. For the microwave-assisted treatment, the pair of bands at 953 and 1020 cm^{-1} may be associated with the characteristic vibrations of the Al–OH bonding. The O–H stretching vibration bands (Ca/Al–OH) can be clearly observed at 3650 and 835 cm^{-1}. The broad peaks at 625 and 2100 cm^{-1} could be due to stretching and bending modes of AlO–(OH) [22]. The broad absorption band in the region 3200–3600 cm^{-1} and the intense bands at 1380 and 1640 cm^{-1} are due to the vibration of H_2O molecules that took part in hydrogen bonding with the Al_2O_3 surface [23]. It is implied that a possible hydrated formation of Ca–Al_2O_3 occurred between mesoporous Al_2O_3 and calcium species during microwave hydrothermal treatment. Additionally, according to the previous report [24,25], FTIR spectra of inorganic aluminates varied with aluminum coordination number, the state of the coordination group (“isolated” or “condensed”) and the vibrational coupling between neighboring groups. The above-mentioned results led to a conclusion that the characteristic absorption regions of Al–O stretching vibrations are 650–800 cm^{-1} for “isolated” and 700–900 cm^{-1} for “condensed” AlO_4 tetrahedra and 400–530 cm^{-1} and 500–680 cm^{-1} regions for “isolated” and “condensed” AlO_6 octahedra. In FTIR spectra, the Al–O stretching vibrations for tetrahedral AlO_4 are observed in the 750–850 cm^{-1} spectral region. At the same time, for octahedral AlO_6, they were observed at 500–750 cm^{-1}. In the OH-stretching region of the FTIR spectrum of the calcined sample, both a sharp peak at 3650 cm^{-1} (Ca–OH and Al–OH bond) and a broad band at 3450 cm^{-1} (H_2O bond) are observed. The FTIR analysis of the calcined sample (M-CaAl) is consistent with the XRD results. Additionally, in order to understand the formation of nanorods–nanotubes, XRD and SEM analyses were performed. The XRD pattern in Fig. 6(c) showed that the as-synthesized samples after microwave hydrothermal treatment exhibited an amorphous crystallite, indicating it could be hydroxylated species (Ca-containing Al_2O_3 matrix). The SEM image in Fig. 6(d) of the as-synthesized sample revealed that no nanorods–nanotubes appeared. The results can provide the evidence

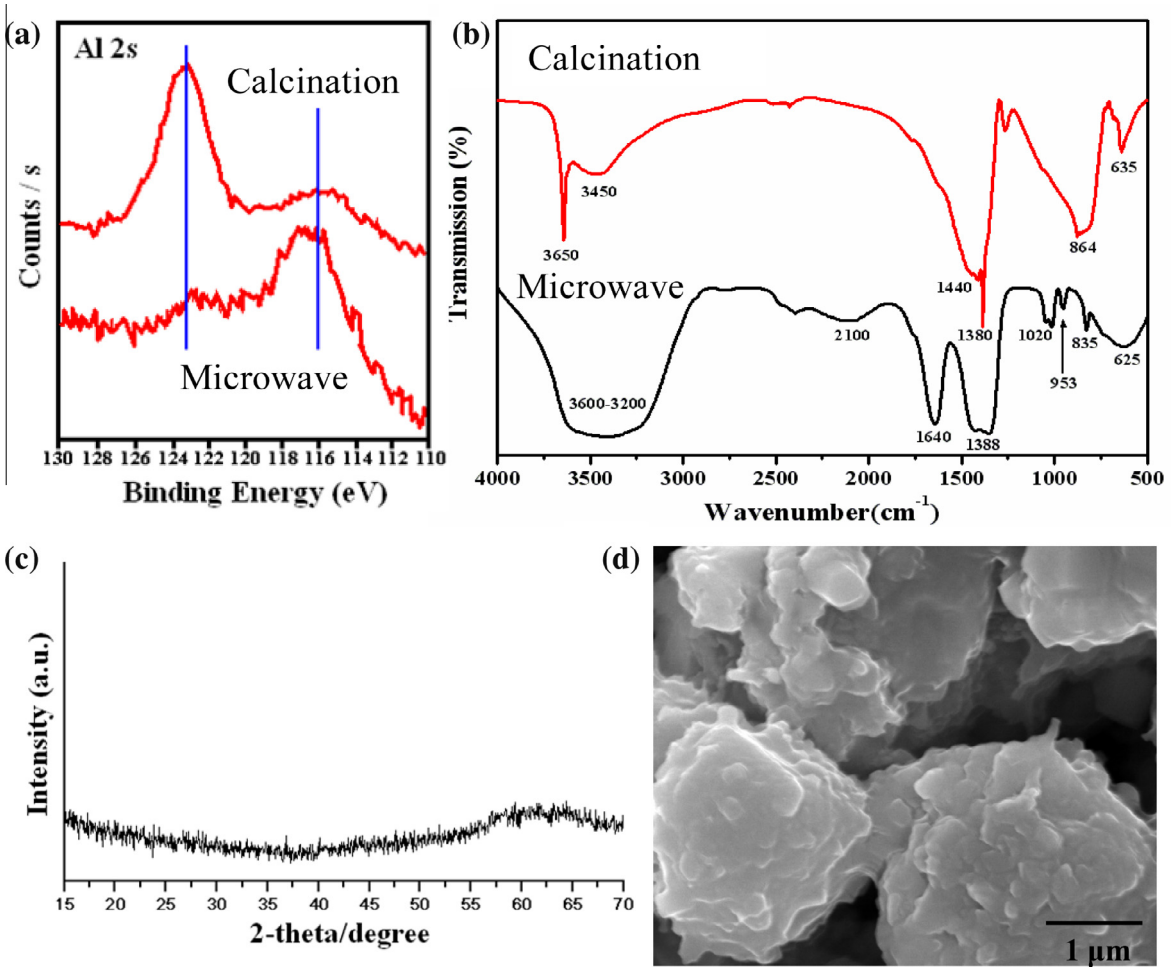

Fig. 6. (a) X-ray photoelectron and (b) FTIR spectra of the M-CaAl sample (Ca/Al ratio = 1) prepared by microwave hydrothermal treatment for 1 h and calcined at 600 °C, (c) large-angle XRD pattern and (d) SEM image of the M-CaAl sample after microwave hydrothermal treatment.

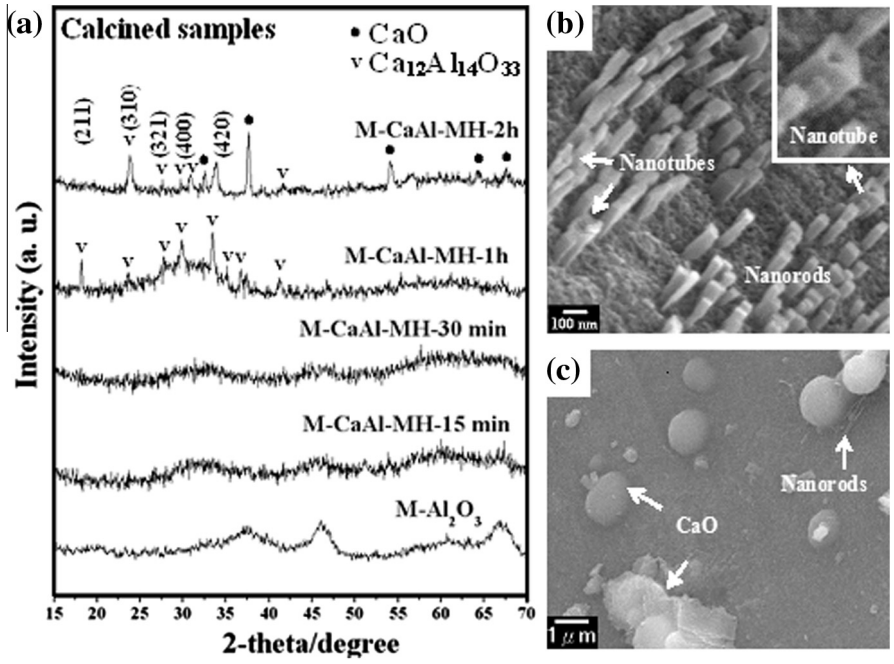

Fig. 7. (a) Large-angle XRD patterns of calcined samples (M-CaAl) with different reactive times at 80 °C during microwave hydrothermal (MH) reaction, followed by calcination at 600 °C, (b) and (c) SEM images of calcined samples (M-CaAl-MH-2 h) taken from two different areas. (*Note*: the prepared M-CaAl sample with Ca/Al ratio = 1.)

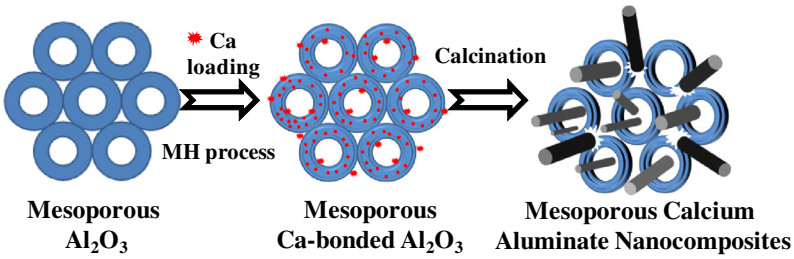

Scheme 1. The formation mechanism of mesoporous calcium aluminate nanocomposites.

that the as-synthesized sample appeared as hydroxylated species after hydrothermal treatment step but would be transformed into nanorods–nanotubes after high-temperature calcinations.

3.3. Formation mechanism of mesoporous calcium aluminate nanocomposites

Fig. 7(a) shows the PXRD patterns of calcined samples (Ca/Al molar ratio = 1) prepared by the microwave assisted process at 80 °C with hydrothermal times ranging from 15 min to 2 h. Firstly, no diffraction peaks were detected in PXRD patterns for samples MH-15 min and MH-30 min, indicating that these samples may exist in a poorly crystalline or amorphous Ca–Al–O solid solution. Upon increasing the microwave hydrothermal time to 1 h, a $Ca_{12}Al_{14}O_{33}$ phase can be clearly detected from the XRD pattern, which is supported by the SEM image in Fig. 3(b) which showed $Ca_{12}Al_{14}O_{33}$ nanorods grown on the mesoporous surface. As the microwave hydrothermal time was extended to 2 h, Fig. 7(b) shows that more nanorods and fewer nanotubes were found to be dispersed on the mesoporous Ca-containing Al_2O_3 matrix, but some aggregative and large CaO particles were also observed in the same sample, as shown in Fig. 7(c). It can be inferred that longer microwave heating times may decrease the attractive force between Ca^{2+} and Al–OH, and some of the calcium ions remaining outside the surface of mesoporous Al_2O_3 rapidly migrated and aggregated to form the larger CaO particles during subsequent calcination, as supported by the PXRD results of Fig. 7(a). On the other hand, if the microwave-assisted reaction was allowed to proceed for more than 3 h, it was found that more crystalline $Ca_{12}Al_{14}O_{33}$ nanotubes may be formed, indicating that growth of the crystalline $Ca_{12}Al_{14}O_{33}$ nanorods or nanotubes varies with microwave reaction conditions.

The formation mechanism of mesoporous calcium aluminate nanocomposites is further illustrated in Scheme 1. The process for the formation of mesoporous Al_2O_3 is based on so-called "evaporation induced self-assembly (EISA)" [26,27]. When subjected to calcination at high temperature (700 °C) to remove the surfactant, a polycrystalline γ-Al_2O_3 structure was formed with an ordered mesostructure and high thermal stability (designated as mesoporous Al_2O_3), which corresponds to the PXRD in Fig. 2(a). As mesoporous γ-Al_2O_3 was used as a support to react with calcium ions in alcohol solution during the microwave hydrothermal reaction, the formation pathway of the $C_{12}Al_{14}O_{33}$ nanorods may be related to Al_2O_3 hydration and a nucleation process between Ca species and Al_2O_3, according to the PXRD, SEM, XPS and FTIR results. In the solution, the mesoporous Al_2O_3 crystallites may be hydrated to form amorphous mesoporous hydrated-Al_2O_3 possessing highly concentrated oxy-hydroxide and hydroxide groups (such as AlO–OH and AlOH) on the Al_2O_3 surface. During the microwave synthesis, Ca ions were attracted and promoted toward the hydrated-Al_2O_3 matrix, depositing inside or outside the surface of the mesoporous hydrated-Al_2O_3 surface and leading to the pre-crystal formation (such as AlO–Ca–OH or $CaAlO(OH)_x$; designated as mesoporous Ca-bonded Al_2O_3). Next, the solid-state reactions (calcinations) could promote the phase transformation of the mesoporous calcium aluminate nanocomposites, in which two types of calcium aluminates (amorphous Ca-containing Al_2O_3 or crystalline $C_{12}Al_{14}O_{33}$ nanorods) could be formed depending on Ca ion content. The Ca-rich pre-crystal complexes inside the mesochannel pore or outside the surface of Al_2O_3 mesochannel could react with more Al_2O_3 nano-frameworks to grow pure $Ca_{12}Al_{14}O_{33}$ nanorods after calcination at high temperature. In contrast, the Ca-poor complexes deposited on the Al_2O_3 surface may be doped into the Al_2O_3 frameworks to form an amorphous Ca–O–Al solid solution. In summary, hydrothermal time and elemental composition (Ca/Al) play important roles in forming mesoporous calcium aluminate nanocomposites via the microwave hydrothermal process.

4. Conclusion

Novel mesoporous calcium aluminate ($Ca_{12}Al_{14}O_{33}$) nanocomposites with nano-scale rods and mesoporous frameworks have been successfully synthesized using the microwave-hydrothermal process and calcination below 600 °C. The mesoporous calcium aluminate nanocomposites possessed a specific surface area of 51 $m^2 g^{-1}$ and a broad pore size distribution of 4–12 nm. The highly dispersed $Ca_{12}Al_{14}O_{33}$ nanorods on the mesoporous frameworks can be obtained by controlling the Ca/Al molar ratio to be 1:1; in such samples, the polycrystalline-like $C_{12}Al_{14}O_{33}$ nanorods were grown in and on the one-dimensional mesochannels. A formation mechanism of the mesoporous calcium aluminate nanocomposites involving amorphous mesoporous hydrated-Al_2O_3 was also proposed. Mesoporous Ca-Al metal oxide materials with highly dispersed $C_{12}Al_{14}O_{33}$ nanorods inside or outside the mesoporous framework could be used to treat natural gas for hydrogen gas production for applications in fuel cells, power plants or fuel combustion in vehicles.

Acknowledgements

The authors gratefully acknowledge the financial support of the National Science Council in Taiwan through Contract NSC-101-3113-E-009-003.

References

[1] F.T. Wallenberger, N.E. Weston, S.D. Brow, Melt Processed Calcium Aluminate Fibers: Structural Optical Properties, Bellingham, Proc. SPIE, 1991.
[2] M. Lacerada, J.T.S. Irvine, E.E. Lachowski, E.P. Glasser, A.R. West, Br. Ceram. Trans. 87 (1988) 191.
[3] M. Sharma, A.A. Khan, K.C. Dohhen, J. Christopher, S.K. Puri, D.K. Tuli, R. Sarin, J. Am. Oil Chem. Soc. 89 (2012) 1545.
[4] A.A. Lemonidou, M.A. Goula, I.A. Vasalos, Catal. Today 46 (1998) 175.
[5] K. Fujji, W. Kondo, H. Ueno, J. Am. Ceram. Soc. 69 (1986) 361.
[6] M. Uberoi, S.H. Risbud, J. Am. Ceram. Soc. 73 (1990) 1768.
[7] M.A. Gulgun, O.O. Popoola, W.M. Kriven, J. Am. Ceram. Soc. 77 (1994) 531.
[8] D.M. Roy, R.R. Neurgaonkar, T.P. O'Holleran, R. Roy, Am. Ceram. Soc. Bull. 56 (1977) 1023.
[9] M.F. Zawrah, N.M. Khalil, Ceram. Int. 33 (2007) 1419.

[10] E.D. Neas, M.J. Collins, Microwave heating, theoretical concepts and equipment design, in: Steven L. Suib (Ed.), Introduction to Microwave Sample Preparation, Theory and Practice, American Chemical Society, Washington, 1993.
[11] D.R. Baghurst, D.M.P. Mingos, J. Chem. Soc. Chem. Commun. 9 (1992) 674.
[12] S.E. Park, D.S. Kim, J.S. Chang, W.Y. Kim, Catal. Today 44 (1998) 301.
[13] B.L. Newalkar, S. Komarneni, Chem. Mater. 13 (2001) 4579.
[14] Q. Yuan, A.X. Yin, C. Luo, L.D. Sun, Y.W. Zhang, W.T. Duan, H.C. Liu, C.H. Yan, J. Am. Chem. Soc. 130 (2008) 3465.
[15] M. Kruk, M. Jaroniec, Chem. Mater. 13 (2001) 3169.
[16] Z. Zhaorong, J. Thomas, Angew. Chem. 120 (2008) 7611.
[17] S.F. Wu, Q.H. Li, J.N. Kim, K.B. Yi, Thermochim. Acta 388 (2002) 105.
[18] J.M. Rivas Mercury, A.H. De Aza, X. Turrillas, P. Pena, J. Solid State Chem. 177 (2004) 866.
[19] P. Gruene, A.G. Belova, T.M. Yegulalp, R.J. Farrauto, M.J. Castald, Ind. Eng. Chem. Res. 50 (2011) 4042.
[20] Z.Y. Yuan, B.L. Su, Chem. Phys. Lett. 381 (2003) 710.
[21] T.Z. Ren, Z.Y. Yuan, B.L. Su, Chem. Phys. Lett. 374 (2003) 170.
[22] P. Colomban, J. Mater. Sci. Lett. 7 (1988) 1324.
[23] G.K. Priya, P. Padmaja, K.G.K. Warrier, A.D. Damodaran, G. Aruldhas, J. Mater. Sci. Lett. 16 (1997) 1584.
[24] P. Tarte, Spectrochim. Acta A 23 (1967) 2127.
[25] G. Arukdhas, Molecular Structure and, Spectroscopy,Prentice-Hall of India Pvt.Ltd, 2008.
[26] Q. Huo, D.I. Margolese, G.D. Stucky, Chem. Mater. 8 (1996) 1147.
[27] P. Yang, D. Zhao, D.I. Margolese, B.F. Chmelka, G.D. Stucky, Nature 396 (1998) 152.